Angle-restricted FWI for shallow reservoir characterisation

Isabel Espin[1]*, Laurene Michou[1], Nicolas Salaun[1], Daniela Donno[1], Øystein Wergeland[2], Katrine Gotliebsen[2], Diego Carotti[1], Joachim Mispel[2] and Ståle Høgden[3]

Abstract

In the Barents Sea, bright amplitudes on seismic data below the Base Quaternary may indicate the presence of hydrocarbon reservoirs. To allow characterisation and quantitative interpretation of these potential reservoirs, analysis of amplitude versus reflection angle (AVA) information is crucial. Even with the availability of high-quality Q-Kirchhoff pre-stack depth migration (QPSDM) products, transmission-absorption relating to shallow gas pockets along with residual surface-related and interbed multiples may compromise the imaging of these shallow reservoirs. By using the full wavefield, imaging from full-waveform inversion (FWI Imaging) provides a reflectivity image without the need to perform the usual pre-processing and migration steps. While FWI Imaging has delivered superior results in terms of imaging compared to more conventional migration methods, it has so far only provided a structural image, without access to common image gathers used to derive AVA information. In this study, we extract elastic information from acoustic FWI Images, generated from impedance updates using angle-restricted raw seismic data. The results of the angle-restricted FWI flow provide comparable AVA products to those obtained from a conventional QPSDM approach and a cleaner and more structurally appropriate AVA image in areas with complex near-surface geology suffering from lack of resolution, noise content or absorption-transmission effects.

Introduction

The Greater Castberg area of the Barents Sea is characterised by a hard water-bottom, at approximately 400 m in depth, followed by a rapid lateral change in geology from west to east, across the Bjørnøyrenna Fault Complex and the Polhem Sub-platform to the Loppa High (Sollid et al., 2021). Overlaying this variable geology, a heterogeneous Quaternary layer was deposited, characterised by the presence of shallow gas pockets, gas hydrates, pockmarks, and iceberg scours. Below the base Quaternary interface, identified as a strong seismic reflector, bright amplitudes suggesting the presence of hydrocarbons can be observed, which can be associated to sandstone reservoir plays located within the faulted blocks, as shown in Figure 1. To understand and delineate these possible reservoirs, analysis of the seismic amplitude versus

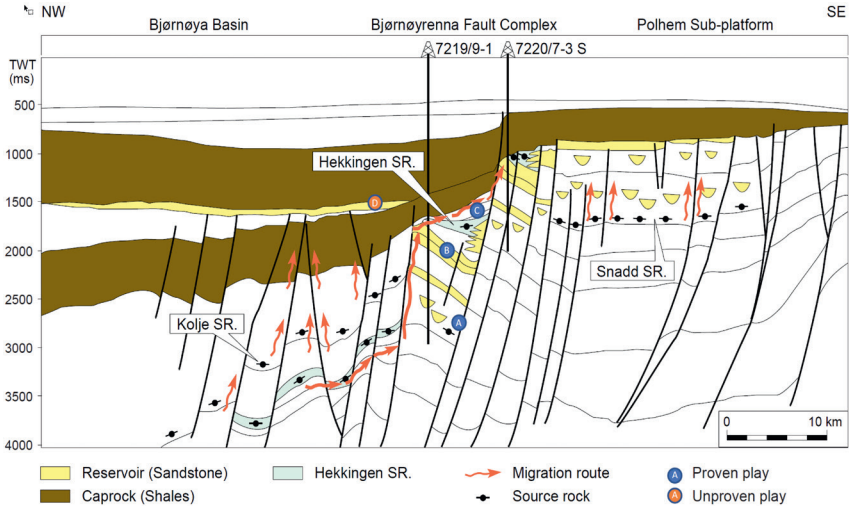

Figure 1 Geological cross section of the Johan Castberg area, illustrating the typical setting for discoveries and prospects sitting along the Bjørnøyrenna Fault Complex (from Sollid et al., 2021, reprinted by permission of the AAPG whose permission is required for further use).

[1] Viridien | [2] Equinor | [3] Vår Energi
* Corresponding author, E-mail: isabel.espin@viridiengroup.com
DOI: 10.3997/1365-2397.fb2024101

reflection angle (AVA) information is crucial (Ostrander, 1984; Gassaway and Richgels, 1983). In 2019, a source-over-streamer (Vinje and Elboth, 2019) dataset was acquired with the goal of obtaining a high-resolution image of the overburden and deeper targets from the Early Jurassic to the Early Cretaceous formations. After this acquisition, an advanced processing and velocity model building sequence was designed to build a 13 Hz visco-acoustic full-waveform inversion (Q-FWI) velocity model and obtain a high-resolution Q-Kirchhoff pre-stack depth migration (QPSDM) (Salaun et al., 2019, 2021). However, imaging of these shallow reservoirs remains challenging as, in addition to the transmission-absorption caused by the shallow gas pockets, surface-related and interbed multiples contaminate the image.

FWI imaging (Zhang et al., 2020) has been successfully applied in the Barents Sea (Espin et al., 2023) to obtain ultra-high-resolution images. By inverting the full wavefield (primary reflections, ghosts, multiples and diving waves), FWI imaging can provide an elegant solution to obtain a reflectivity image without having to perform the usual pre-processing and migration steps. The resulting image demonstrates an improved signal-to-noise ratio (SNR) as well as continuity and focusing of the events when compared to conventional imaging methods. However, acoustic FWI Imaging lacks the ability to access the AVA or elastic information needed to properly characterise reservoirs and perform quantitative interpretation. One possible solution would be to employ elastic FWI to invert for Vp and Vs. This is particularly true in the case of a multi-sensor recording system, such as ocean-bottom nodes, where pressure and shear wave velocity can be properly decoupled thanks to the recording of vertical and horizontal components (Masmoudi et al., 2024). However, this inversion might be poorly constrained due to the nature of the available acquired towed-streamer data. Another solution is to extract elastic information through acoustic FWI, as proposed by Warner et al. (2022). AVA information can be retrieved by running several acoustic FWIs using angle-restricted raw seismic data as an input. In this paper, we describe how a high-resolution and angle-restricted acoustic FWI flow can be applied to successfully image and characterise shallow reservoirs.

FWI imaging to resolve imaging challenges

Despite the high quality of the conventional processing applied to our study area (Poole et al., 2020), the use of primary energy alone does not allow optimal imaging of the subsurface, particularly the near surface. To improve the imaging, we performed a FWI velocity update up to a maximum frequency of 150 Hz (Figure 2c) inverting the full wavefield (primary reflections, ghosts, multiples and diving waves), which allowed retrieval of detailed high-resolution velocity variations between the various geological layers. The corresponding 150 Hz FWI image increased both the resolution and the SNR of the subsurface (Figure 2b) compared to the legacy QPSDM (Figure 2a). The FWI image revealed fine structures undetectable on the conventional QPSDM result and helped with the understanding and delineation of the subsurface.

While this improved image is expected to enhance reservoir understanding, it could also be of great interest for near-surface characterisation and for shallow hazard detection. One of the goals of shallow hazard surveying is to ensure that drilling will not cross a gas pocket in the first few hundred metres below the surface. Dedicated site surveys are often conducted in order to image the specific area with high resolution to spot possible drilling hazards in the very near surface. By using the full recorded wavefield, FWI imaging can increase the resolution of the images and can be used for shallow hazard detection with the benefits of the 3D imaging (Dinh et al., 2023).

The benefits of near-surface imaging can be observed in Figure 3, where the image is focused on the water bottom and the first hundred metres below. As for the previous observations, with the full wavefield, imaging of the fault is dramatically improved (Figures 3a, 3d), showing possible continuity of the fault up to the surface seabed. The auto-tracking of the water bottom performed over the two volumes (Figures 3b, 3e) illustrates the increased resolution of the FWI image. A clear map of the rugous and structured water bottom in this region would be of great help to plan surface installations and drilling. In our case, we chose to display the minimum amplitude along the base Quaternary coming from both conventional and FWI imaging (Figure 3c, 3f). In both cases, gas pockets can be reasonably well detected with this method, but the increased resolution observed on the FWI image is still visible on this map. Gas pockets appear sharper and smaller possible pockets are now visible. These gas pockets present along the Base Quaternary create seismic imaging problems for underlying targets. Indeed, this strong impedance contrast tends to reflect a large part of the emitted signal, reducing the SNR below these events. These

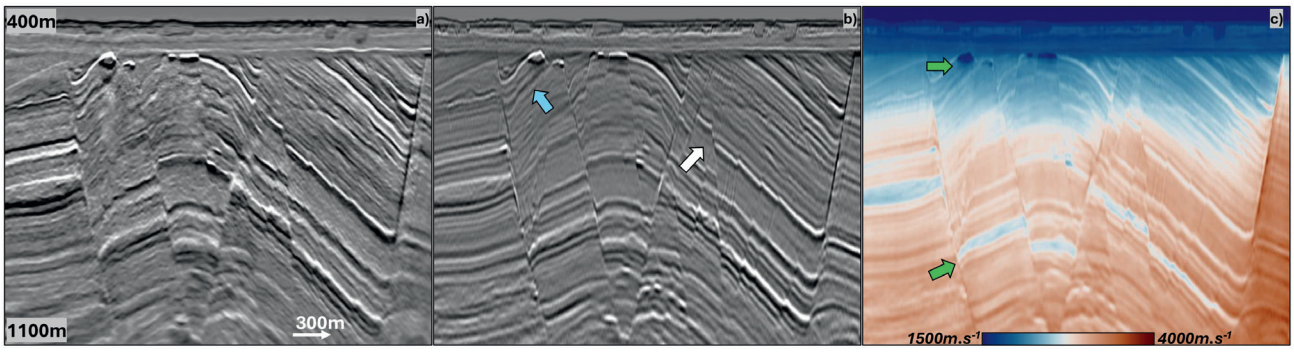

Figure 2 Comparison of a) legacy QSPDM image, b)150 Hz FWI image and c) 150 Hz FWI velocity. FWI imaging improved event continuity (blue arrow) and fault definition (white arrow). Thin-layer velocity slowdown highlights possible changes in rock property or fluid content (green arrows).

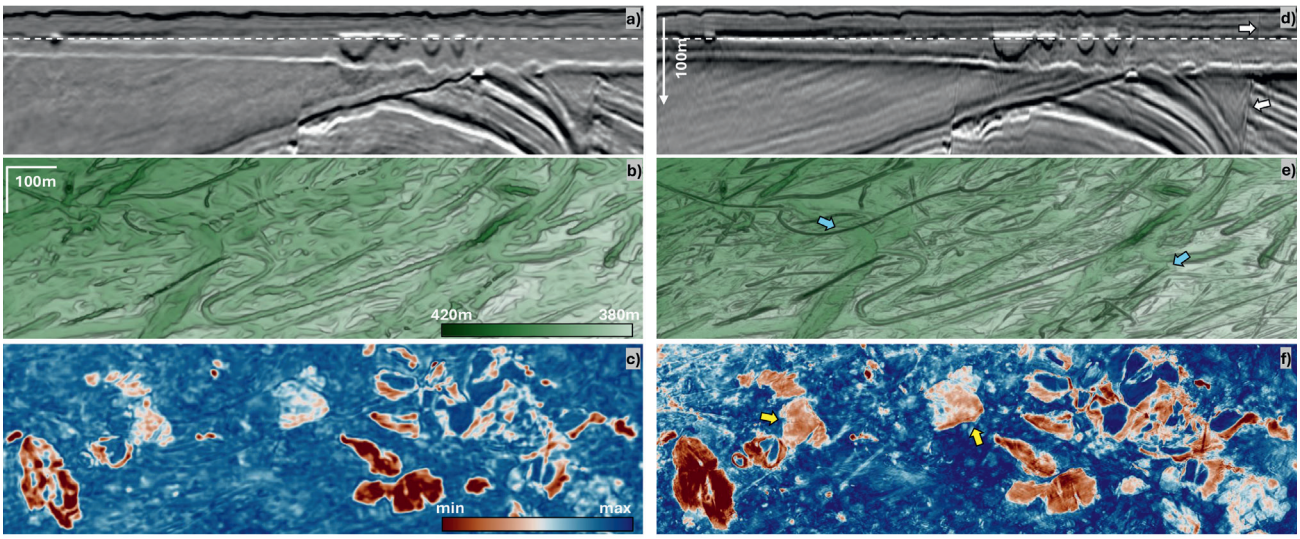

Figure 3 Comparison of legacy QPSDM image and 150 Hz FWI image for a shallow cross-section (a, d), picked water bottom horizon (b, e) and minimum amplitude map within the Quaternary layer (c, f). Depth of the maps c and f are shown by the dashed line on Figures a and d. On the FWI Image, near-surface faults are more visible (white arrows). The associated picked water bottom shows iceberg scours (blue arrows) that are not visible with conventional imaging. When focusing on the amplitude map, FWI imaging improves gas pocket delineation (yellow arrows), facilitating improved potential hazard detection.

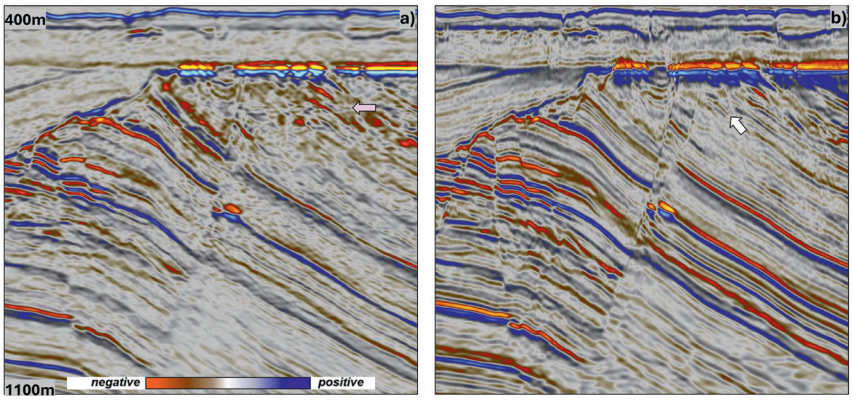

Figure 4 Comparison of a) legacy QPSDM image, b) 150 Hz FWI Image below a gas pocket accumulated along the Base Quaternary. The pink arrow exhibits the presence of an internal multiple bouncing between the water bottom and the gas pocket which interferes with the QPSDM image, but is correctly modelled by the FWI and hence not visible in b) (white arrow).

gas accumulations are also strong internal multiple generators, along with the hard and rugose water bottom.

The sections in Figure 4 illustrate this problem. On Figure 4a, from the legacy QPSDM, the poor SNR and internal multiples are indicated by the pink arrow. These internal multiples, that are not always obvious and depend on the varying impedance contrast of the gas, can be misleading and interpreted as a possible flat spot. FWI imaging naturally accommodates the modelling of internal multiples, and is therefore an excellent tool for confirming or dispelling the presence of flat spots in such an area and ensures the same interpretation quality all along the seismic sections. On Figure 4b, showing the FWI image, continuity below the gas pocket is clearly better and confirms the absence of flat spots. This is critical in this case, as possible reservoirs could be located at similar intervals where these multiples are present in the image, as indicated in Figure 1.

In this example, the structural image appears to be sufficient to define the presence or absence of a possible reservoir. However, having access to elastic information via amplitude-versus-angle information is often of great importance to further characterise reservoirs. To complement information provided with the FWI image, an angle-restricted FWI was performed.

Angle-restricted FWI

The first element for the angle-restricted acoustic FWI is the initial velocity model. In our case, the 150 Hz FWI velocity model obtained with the full-angle data and full wavefield was filtered at 100 Hz and used as input in a 100 Hz acoustic angle-restricted FWI. The second element is the separation of the recorded data into three angle ranges: near 5°-15°, mid 15°-25° and far 25°-35°. These angles are based on 3D ray-tracing using the initial model. Similar to the full-offset FWI, we start from the raw shot records. The same wavelet, extracted from the data, was used for the three independent inversions. In contrast to the method proposed by Warner et al. (2022), and in the context of this study, we invert for impedance rather than velocity. Initial impedance was calculated from the inverted 150 Hz velocity model filtered to 100 Hz and density estimated from the Gardner relationship.

To evaluate the quality of the inversion, modelling was performed with the initial FWI velocity and density models (Figure 5b) and compared with the updated angle-restricted models (Figure 5c). The analysis focused on a known reservoir, located at approximately 700 m depth. Despite the hard water bottom reflector, which generated strong ghosts and multiples, the reflection event associated with the reservoir was visible on the shot gather (green arrows in Figure 5a). The initial velocity

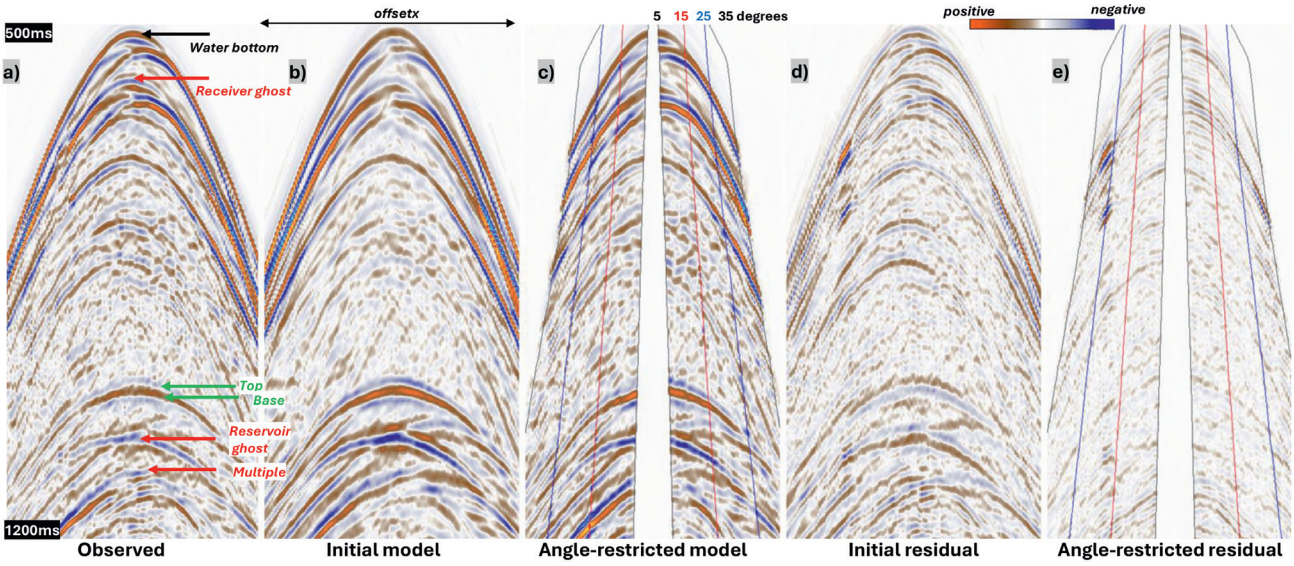

Figure 5 100 Hz FWI modelled shot and residual over a known reservoir to assess the quality of the angle-restricted acoustic FWI. a) Observed shot, b) modelled shot with starting FWI model and its residual in (d); c) modelled shot with 100 Hz angle-restricted FWI update, one impedance model per angle range, and its residual in (e).

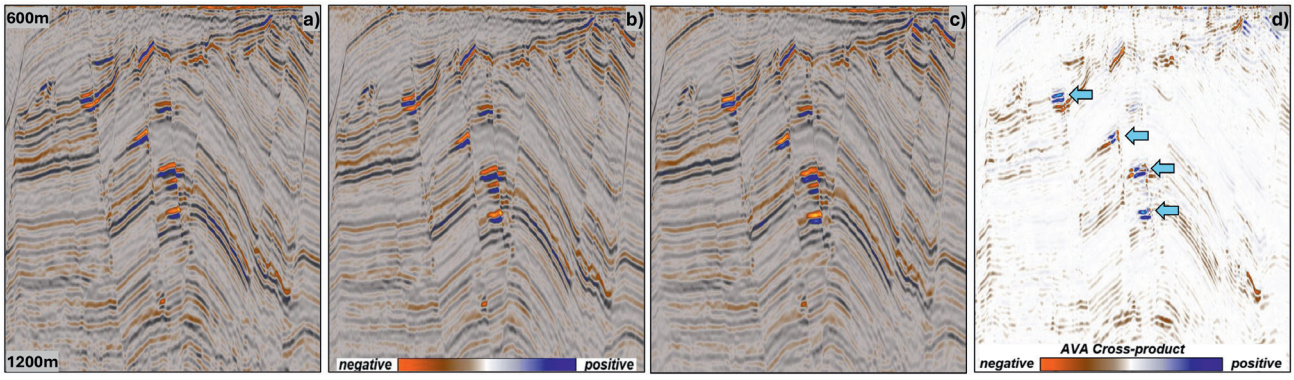

Figure 6 FWI sub-images for the near (a), mid (b) and far (c) angle range. AVA behaviour can be assessed by deriving cross-products between the intercept and gradient. On this cross-product, bright spots are clearly visible, indicated by the blue arrows.

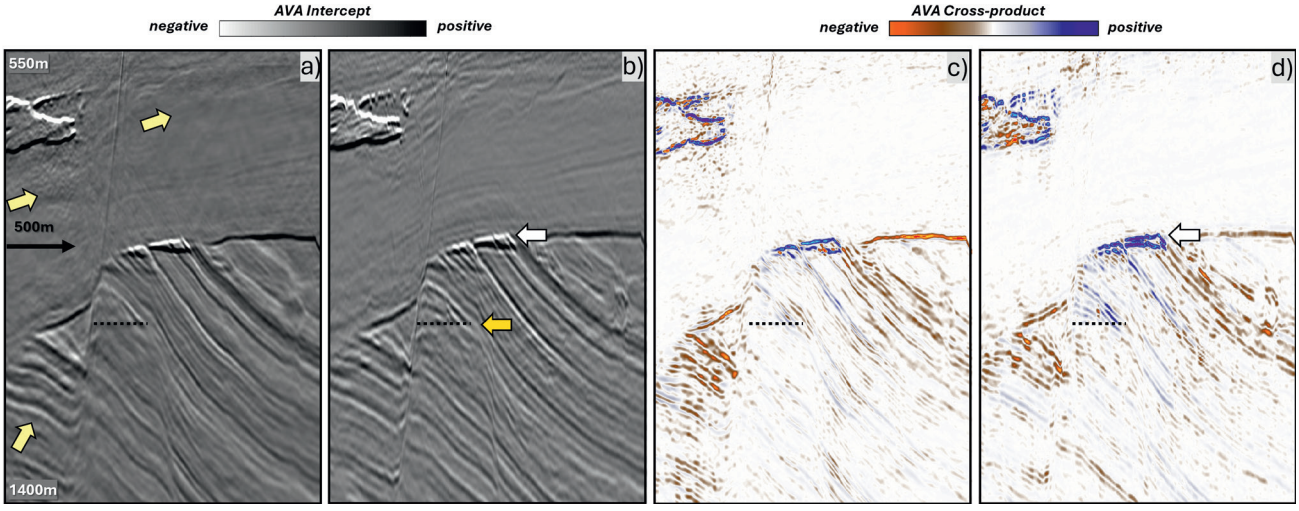

Figure 7 Comparison of the intercept and intercept-gradient cross-product between QPSDM (a and c, respectively) and angle-restricted acoustic FWI (b and d, respectively) at 100 Hz. The FWI-based intercept exhibits improved resolution and fault continuity. A similar trend, in terms of AVA anomalies, is observed between the QPSDM and the FWI result.

and density models allowed modelling of the various events with accurate kinematics, as seen in Figure 5b. However, they lacked accuracy in terms of amplitude fidelity, as observed with the residual (Figure 5d). This amplitude-related residual was as expected because only the starting velocity model was obtained from a previous FWI, the starting density model having been derived from the corresponding Gardner's relationship. When inverting for impedance using FWI on each angle range

separately (Figure 5c), both the kinematic and amplitude matching of the modelled data with the observed data were improved.

The impedances obtained from the angle-restricted FWI were then converted to reflectivity by performing the derivative of the impedance with an angle compensation, which applied the required AVA correction to the angle-restricted acoustic FWI Images (Warner et al., 2022). We hence obtained three FWI sub-images for the near, mid and far-angle range (Figure 6a, 6b, 6c). These sub-images not only have the benefits of the FWI Image, namely the sharp faulting and the improved SNR, they also preserve the AVA behaviour. To assess the quality of the results, AVA attributes, such as intercept, gradient and cross-product, can be computed from the FWI sub-images, as performed in Figure 6d. We can appreciate here the presence of small hydrocarbon pockets sitting along the faults and their amplitude increasing as the incidence angle increases.

To validate the AVA information obtained from our FWI sub-images, the intercept and cross-product were also compared with the legacy QPSDM (Figure 7). The structural uplift observed with the full-angle FWI Image was preserved, fault networks were sharper and the shallow gas pockets were better captured. Regarding reservoir characterisation, the class 3 AVA was captured for this known gas reservoir (Figure 7d). Analysing Figure 7, AVA trends were quite similar between the angle-restricted FWI and the QPSDM, even in the deeper part of the section, below the arrival of the first-order surface-related multiple.

After confirming the good match in AVA behaviour between the well-established PSDM and our proposed angle-restricted FWI method, another assessment was made, this time in the Nordkapp basin, also in the Barents Sea, where a gas accumulation is visible as strong bright amplitudes in the FWI image.

For this test, a model-based stratigraphic inversion was run using the FWI sub-images, which were derived with the same angle-restricted FWI workflow as explained before. In this case, the process inverted simultaneously the different FWI sub-image reflectivity obtained for the different angles using the same starting model used for the angle-restricted FWI as input (Coulon et al, 2006). During inversion, the initial model is iteratively perturbed using a simulated annealing procedure to find a global solution that optimises simultaneously the match between the input sub-images and the corresponding synthetics, calculated by convolution using the full Zoeppritz reflectivity equations. The Vp and Vs properties obtained after the inversion correspond, as expected, to a class 3 AVA anomaly (Figure 8), with a slow-down in the gas pocket for Vp while no fluid effect was visible for the Vs. This confirmed the good decoupling of the Vp and Vs estimation and hence the quality of the FWI sub-Images to conduct further reservoir characterisation.

Acoustic FWI for AVA: benefits and limitations

The benefits of angle-restricted FWI are particularly visible when conventional imaging tools, such as Kirchhoff migration, struggle to image the reflectors. Sub-optimal imaging results obtained by conventional methods can be attributed to different reasons, such as the complexity of the raypaths, lack of resolution, transmission, absorption, noise or signal leakage during the conventional data pre-processing. This is illustrated in Figure 9, where the QPSDM (Figures 9a and 9c) shows a possible reservoir affected by the presence of a shallow gas pocket in the overburden. The

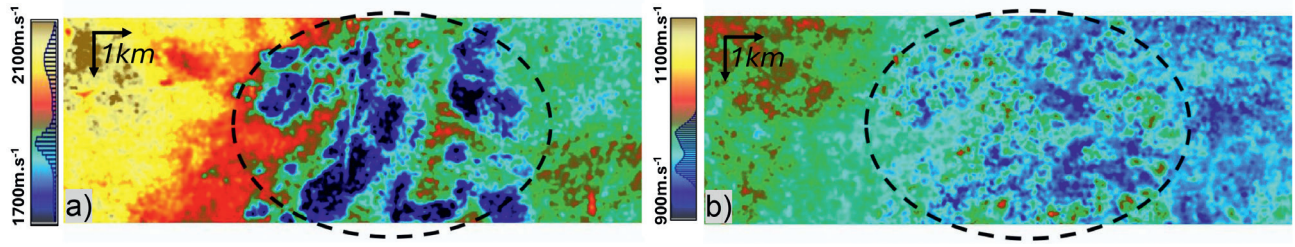

Figure 8 A model-based stratigraphic inversion was conducted over a shallow gas pocket, in the Nordkapp Basin, using angle-restricted FWI Images as input. Depth slice view illustrates the obtained Vp (a) and Vs (b). As expected, a slow-down of Vp was observed within the gas pocket, while it is absent in the inverted Vs. Courtesy of AkerBP.

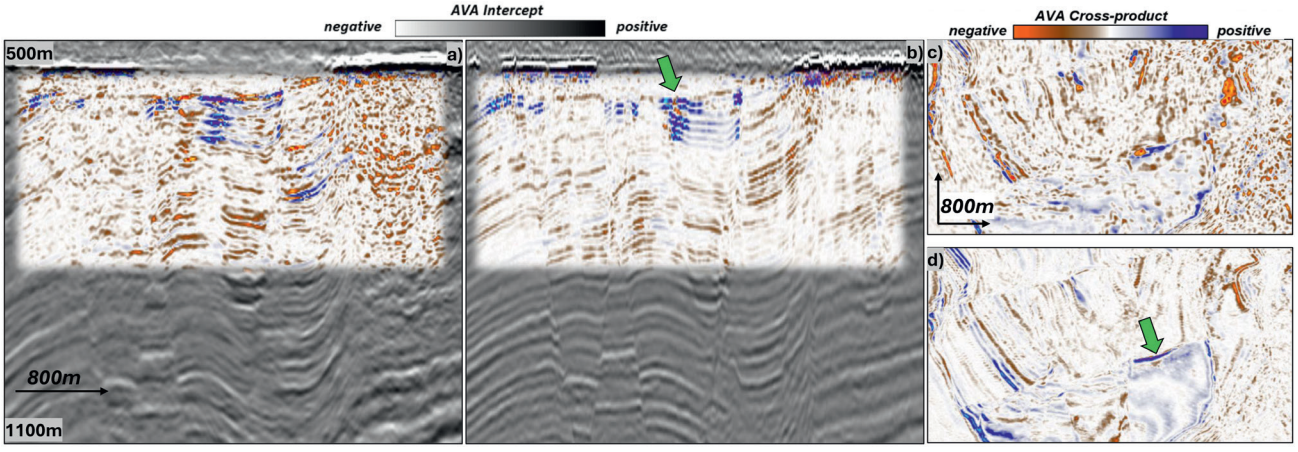

Figure 9 Comparison of intercept-gradient cross-product, overlaid with intercept for subline view, QPSDM (a) and angle-restricted acoustic FWI (b), over a shallow gas pocket. Improved continuity vertically and laterally is observed in the FWI case (green arrows), showing sharp boundaries at the fault planes. Similar observations can be made in the corresponding depth slice view at approximately 575 m (c and d), with improved coherency and reduced noise.

lack of resolution and absorption compensation in the near surface prevents the migration operator from collapsing the diffractions at the location of the faults, which appear smeared, thus compromising the imaging of possible hydrocarbon traps. The AVA cross-product obtained with the FWI flow (Figures 9b and 9d) exhibited a remarkably improved result in this shallow area. The FWI flow also had the benefit of starting from raw recorded data, reducing possible signal leakage or bias in the data processing stage.

Regarding the limitations of this method, it is important to consider that the angle mutes applied to the data are based on the incidence angle of the primary reflection, which is not valid for multiples. This means that the FWI Image for a given angle range would need to satisfy the amplitudes for both the primary reflection angle and the typically smaller multiple reflection angle. As both amplitudes, primary and multiple, cannot be solved at the same time because they correspond to different angles, there is a risk of primary amplitudes not being fully respected. In the case of this study, despite the limitations, results deeper than the multiple arrival depth (around 1.2 km depth) seemed to preserve the expected AVA response compared to the QPSDM result, suggesting that we can qualitatively identify the AVA anomalies. However, this method is particularly recommended for shallow reservoir characterisation, and results deeper than the multiple arrival depth must be interpreted with caution. Angle-restricted FWI could then be a complement to the FWI image used for shallow hazards, refining understanding of the near surface and providing more reliable information about potential drilling hazards.

Conclusions

In the complex geological context of the Barents Sea, three angle-restricted FWI's were run to generate three angle reflectivities, for near, mid and far angles. With this methodology, high-resolution elastic information revealing the expected class 3 AVA response can be derived directly from raw data without the need for a full conventional processing and imaging sequence. Analysis of these results showed comparable amplitude variations between angle stacks obtained with acoustic FWI and with the conventional flow. Cross-product QCs extracted from the FWI sub-images showed a good coherence with the expected results observed from the QSPDM. Benefits of the angle-restricted FWI were observed where the conventional Kirchhoff migration struggled to provide a sharp image due to lack of resolution, noise content or absorption-transmission effects caused by the presence of shallow gas pockets. In these cases, high-frequency FWI imaging delivered a more detailed, cleaner and more structurally appropriate image than the conventional imaging approach due to the use of the full wavefield and more accurate solving of multiples.

Acknowledgements

We would like to thank Equinor, Vår Energi, Petoro, TGS and Viridien for permission to publish these results. We thank AkerBP for permission to show/publish the Nordkapp basin example. We also thank our colleagues Jean-Philippe Coulon and Bernard Deschizeaux for useful discussions.

References

Coulon, J.-P., Lafet, Y., Deschizeaux, B., Doyen, P.M. and Duboz, P. [2006]. Stratigraphic elastic inversion for seismic lithology discrimination in a turbiditic reservoir. *SEG Expanded Abstract*, 2092-2096.

Dinh, H., Latter, T., Townsend, M., and Grinde, N. [2023]. Dual-azimuth FWI imaging and its potential in shallow hazard assessment. *84th EAGE Annual Conference & Exhibition*, Extended Abstract.

Espin, I., Salaun, N., Jiang, H. and Reinier, M. [2023]. From FWI to ultra-high-resolution imaging. *The Leading Edge*, **42**(1), 16-23.

Gassaway, G.S. and Richgels, H.J. [1983]. SAMPLE, seismic amplitude measurement for primary lithology estimation. *53rd SEG meeting*, Expanded Abstracts, 61G 613.

Masmoudi, N., Ratcliffe, A., Bukola, O., Tickle, J. and Chen, X., [2024]. Elastic FWI of Multi-Component Ocean-Bottom Seismic to Update Shear-Wave Velocity Models. *85th EAGE Annual Conference & Exhibition*, Extended Abstract.

Ostrander W.J. [1984]. Plane wave reflection coefficients for gas sands at nonnormal angles of incidence. *Geophysics*, **49**, 1637-1648.

Poole, G., Cichy, K., Kaszycka, E., Vinje, V. and Salaun, N. [2020]. On top of seismic sampling-benefits of high-resolution source-over-streamer acquisition. *82nd EAGE Annual Conference & Exhibition*, Extended Abstract.

Salaun, N., Henin, G., Wright, A., Pellerin, S., Deprey, J., Deschizeaux, B., Souvannavong, V., Dhelie, P. and Danielsen, V. [2019]. Capturing the value of high-resolution source-over-streamer acquisition at Barent Sea. *81st EAGE Annual Conference & Exhibition*, Extended Abstract.

Salaun, N., Reinier, M., Espin, I. and Gigou, G. [2021]. FWI velocity and imaging: A case study in the Johan Castberg area. *82nd EAGE Annual Conference & Exhibition*, Extended Abstract.

Sollid, K., Henriksen, L. B., Hansen, J. O., Thießen, O., Ryseth, A., Knight, S., & Groth, A. [2021]. Johan Castberg: the first giant oil discovery in the Barents Sea. *AAPG Memoir 125: Giant Fields of the Decade: 2010–2020*, Robert K. Merrill and Charles A. Sternbach, eds., 213–248.

Vinje, V. and Elboth, T. [2019]. Hunting high and low in marine seismic acquisition; combining wide-tow top sources with front sources. *81st EAGE Annual Conference & Exhibition*, Extended Abstract.

Warner, M., Armitage, J., Umpleby, A., Shah, N., Debens, H. and Mancini, F. [2022]. AVO Determination Using Acoustic FWI. *83rd EAGE Annual Conference & Exhibition*, Extended Abstract.

Zhang, Z., Wu, Z., Wei, Z., Mei, J., Huang, R. and Wang, P. [2020]. FWI Imaging: Full-wavefield imaging through full-waveform inversion. *90th SEG Annual International Meeting*, Expanded Abstract, 656-660.